

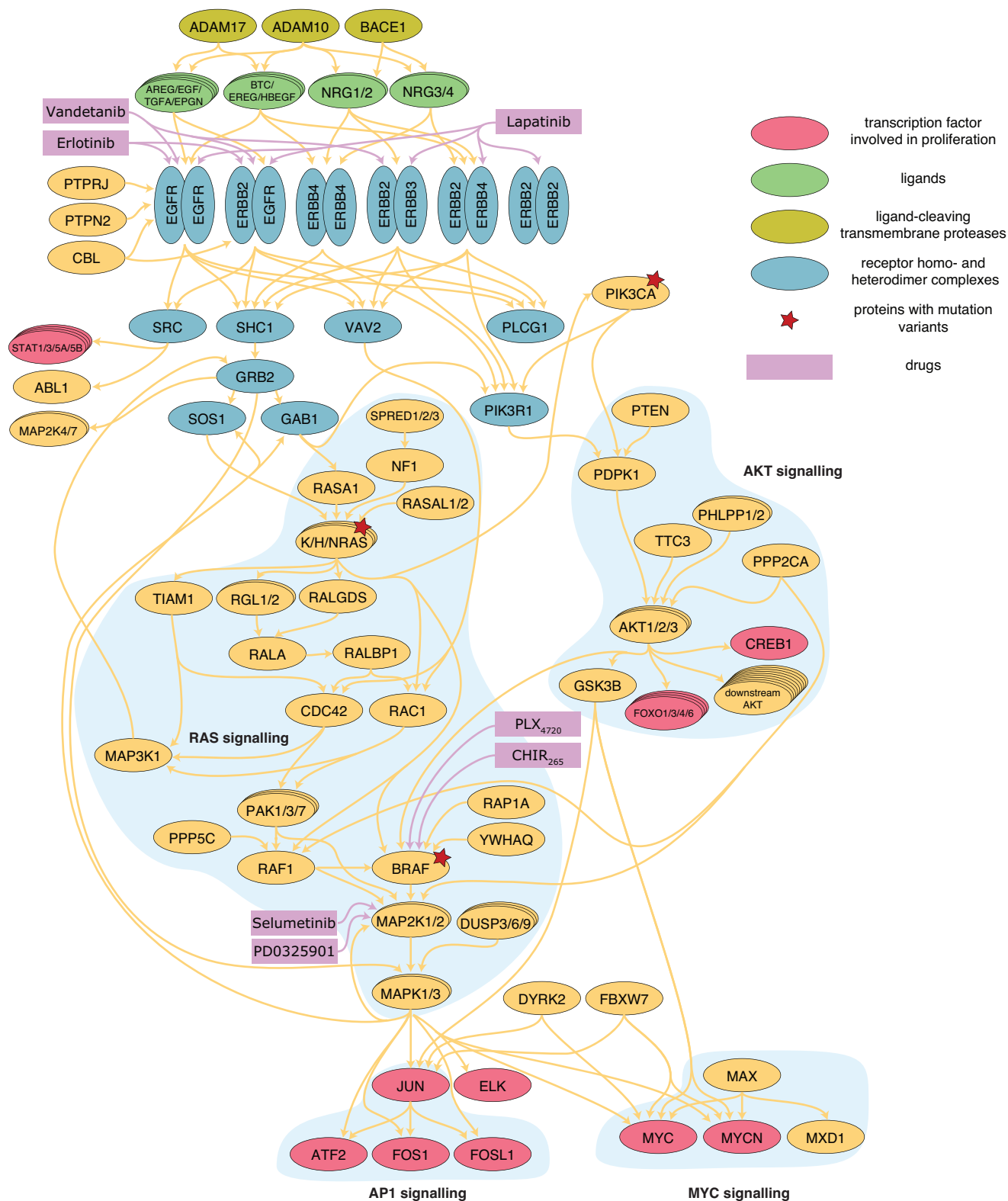
Supplemental Information

Efficient Parameter Estimation

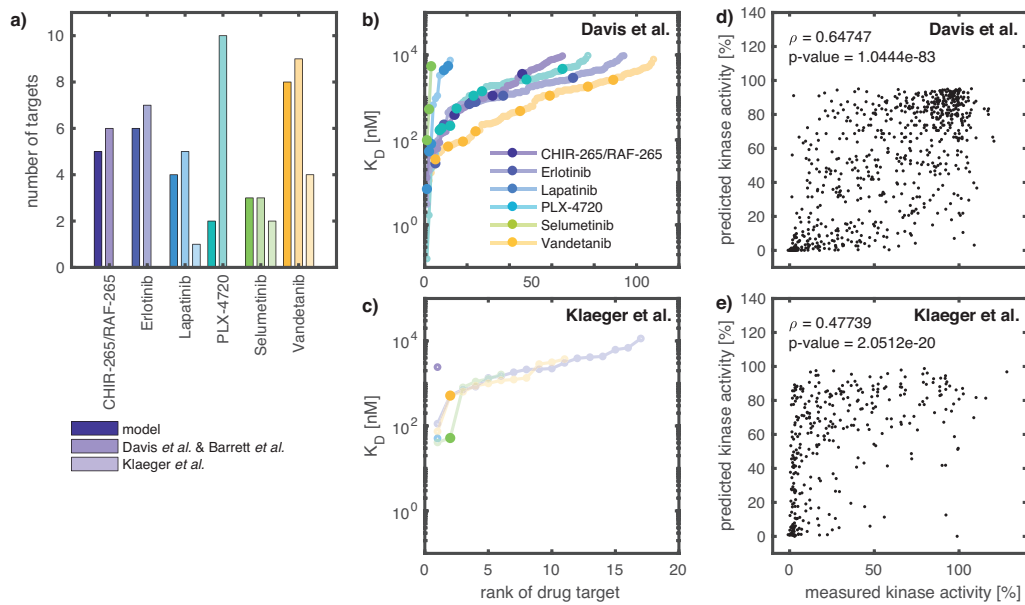
Enables the Prediction of Drug Response

Using a Mechanistic Pan-Cancer Pathway Model

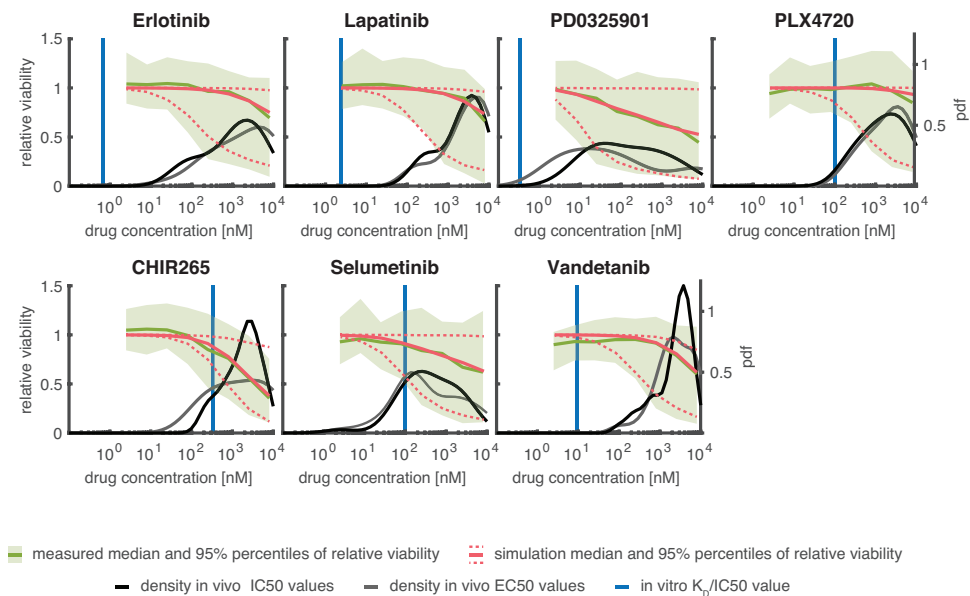
Fabian Fröhlich, Thomas Kessler, Daniel Weindl, Alexey Shadrin, Leonard Schmiester, Hendrik Hache, Artur Muradyan, Moritz Schütte, Ji-Hyun Lim, Matthias Heinig, Fabian J. Theis, Hans Lehrach, Christoph Wierling, Bodo Lange, and Jan Hasenauer



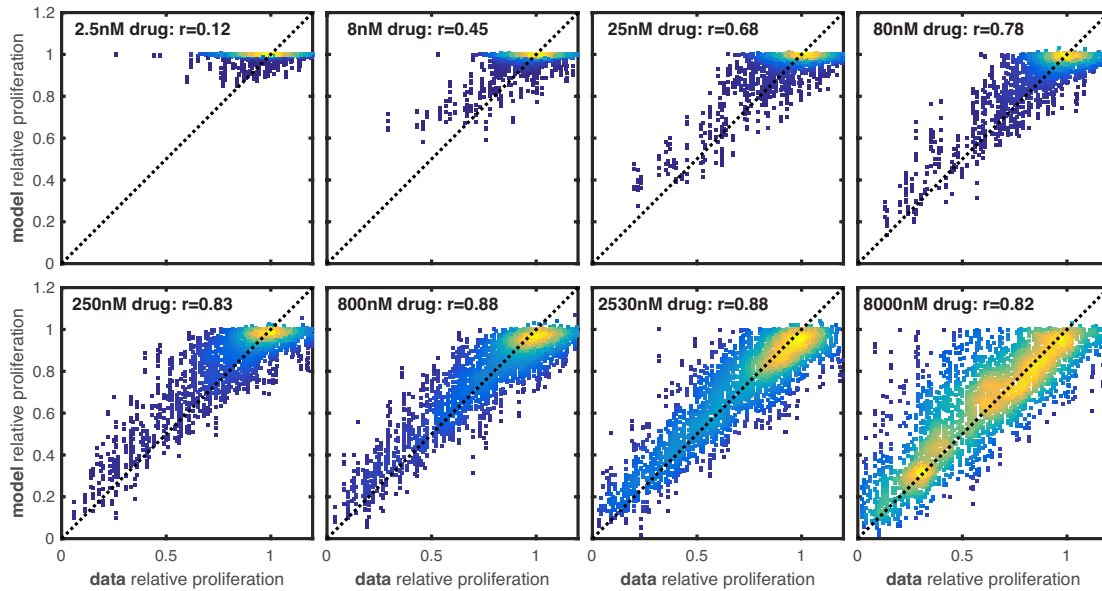
Supplementary Figure S1. Simplified overview of the model, Related to Figure 1. The figure illustrates modeled interactions. Complex formation and phosphorylation as well as activation and repression are not discriminated here. Synthesis, translocation and degradation are omitted. All species are colored according to their function.



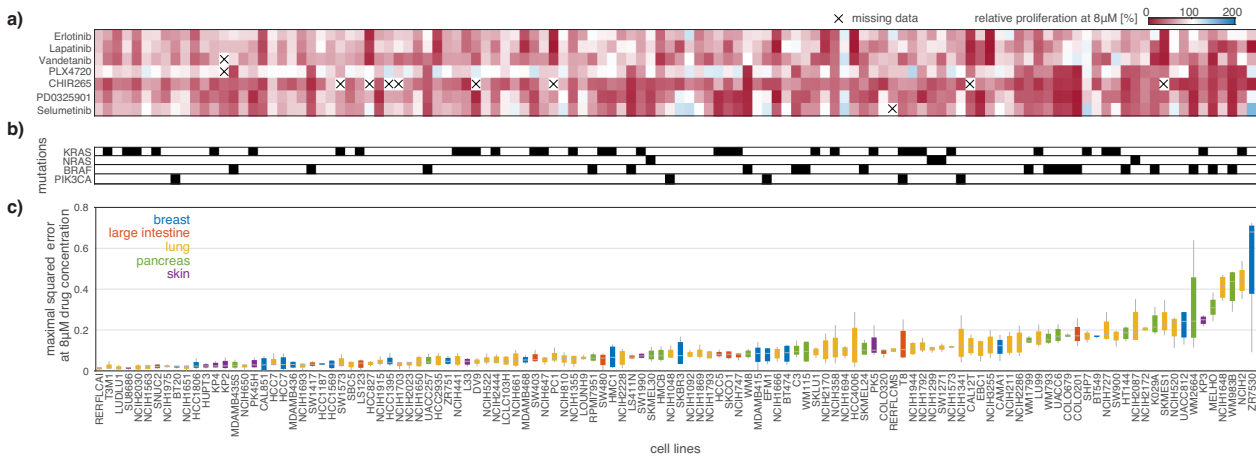
Supplementary Figure S2. Drug-target interaction, Related to Figure 1. (a) Number of drug-target interactions in the canonical human ERBB, RAS and PI3K/AKT cancer signaling pathways. The drug-target interactions observed by Davis *et al.* (2011), Barrett *et al.* (2008) and Klaeger *et al.* (2017), and the drug-target interactions implemented in the mechanistic model are illustrated. (b,c) Spectrum of K_D values reported by Davis *et al.* and Klaeger *et al.* for the considered drugs. Large circles indicate the drug-target interactions implemented in the model. If multiple measured K_D values were reported for a gene (e.g. multiple phosphorylated forms of the kinase or mutations), the mean K_D value is reported. (d,e) Comparison of kinase activities measured by Anastassiadis *et al.* (2011) and kinase activities predicted based on K_D values measured by Davis *et al.* and Klaeger *et al.*. Anastassiadis *et al.* measured the relative kinase activity at 500 nM of the inhibitor. The prediction is obtained using the standard binding model, Kinase + Inhibitor \leftrightarrow Kinase:Inhibitor, yielding relative kinase activity = $K_D / ([\text{inhibitor concentration}] + K_D)$. The scatter plot reports results for all drug-gene pairs which overlap between the respective datasets.



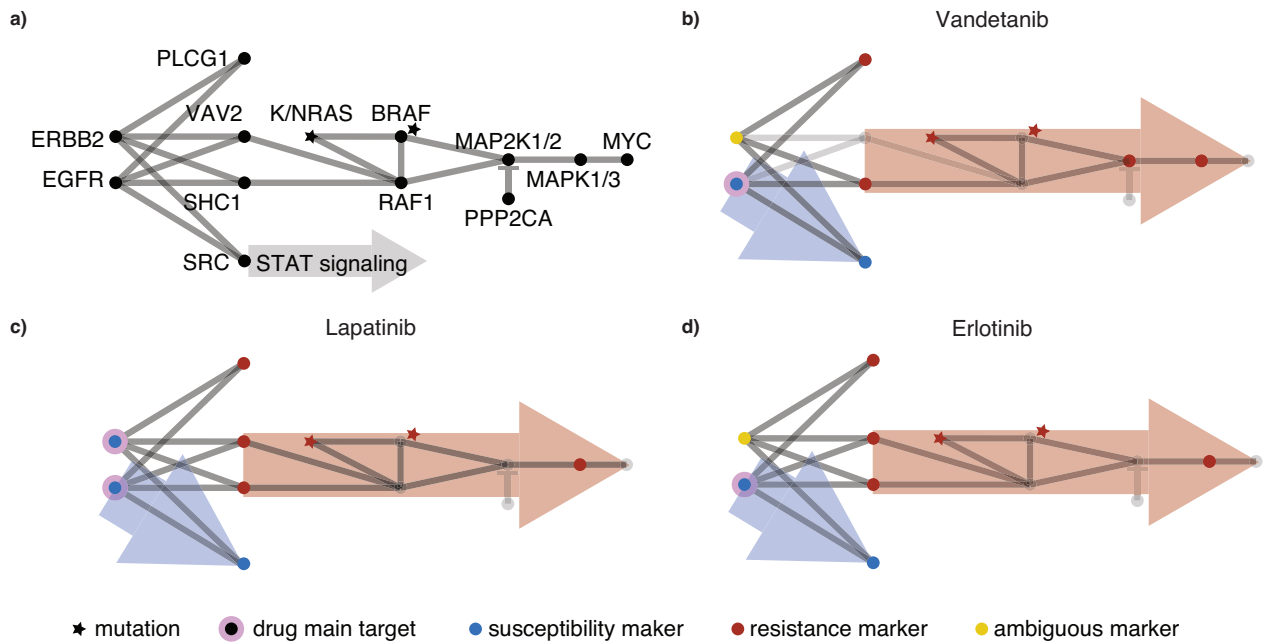
Supplementary Figure S3. Experimentally measured and simulated dose response profiles and in vitro measured K_D /IC50 values, Related to Figure 4. Median measured (green) and simulated (red) relative viability are depicted as solid lines with 95% intervals as shaded area or dotted line across all 120 cell-lines in the training/test set. Density plots of respective IC50 (grey) and EC50 (black), according to CCLE postprocessing, are depicted as solid lines. In vitro measurements of K_D /IC50 values for main targets of all drugs are depicted as horizontal blue line.



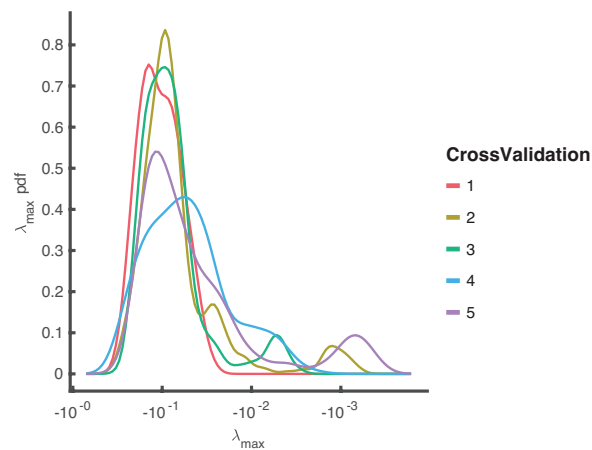
Supplementary Figure S4, Related to Figure 4. Correlation of model simulation and experimental data at all measured drug concentrations. The correlation for the drug concentrations from 250nM to 2530nM is higher than at 8000nM, which may be due to an inflation of cell lines not responding to drugs at low concentrations (relative viability=1). For the drug concentrations from 2.5nM to 80nM the correlation is lower than at 8000nM, which is likely due to the lower dynamic range of simulated and experimentally observed relative viability.



Supplementary Figure S5. Overview of parameterization results, Related to Figure 4. One column corresponds to an individual cell line. The cell lines are sorted according to the median over cross-validations of the maximal squared error at 8µM drug concentration shown in c). (a) Measured relative viability in response to the treatment with 8µM of the different drugs. (b) Gain-of-function mutations in the individual cell lines. Mutation status is summarized per gene and does not distinguish individual variants. (c) Boxplots of the maximal squared error at 8µM drug concentration over the cross-validations. The squared error is evaluated for the median of the simulation from the 5 best optimization runs. The maximum is taken over all drugs. The boxplots are colored according to the tissue of origin of the cell lines.



Supplemental Figure 6. Skeletal structure of drug susceptibility and resistance signaling, Related to Figure 6. (a) Global signaling skeletal structure reconstructed by aggregating the 15 most pronounced susceptibility and resistance markers from all drugs. Connections were reconstructed according to projected model Jacobian. Stars indicate mutation variants. Nodes and stars may aggregate multiple isoforms or mutation variants. (b-d) Drug specific skeletal structure, genes/proteins not in top 15 as well as corresponding connections are greyed out. Arrows indicate resistance (red) and susceptibility (blue) pathways.



Supplementary Figure S7. Linear Stability Analysis, Related to STAR Methods. The distributions include the maximal eigenvalues of the model Jacobian in steady state for all no treatment conditions for parameters from the five best performing optimization runs.

Supplementary Table S1. Polypharmacology implemented in proposed model, Related to Figure 1. Drug interactions implemented in the model compared to experimentally determined drug binding partners in Klaeger et al., 2017 and Davis et al., 2011. The table lists gene symbols and protein names for kinases included in the mechanistic model along with their dissociation constants (K_D) used in the model and as measured in previous studies. For Klaeger et al., 2017, “n.i.” indicates the protein was detected, but no inhibition was observed, and “n.d.” indicates the protein has not been observed. For Davis et al., 2011, “n.d.” indicates the protein was not included in the screening, “n.i.” means no inhibition was observed; “X” indicates that the drug was not included in the screening. In the model column, “--” indicates that the corresponding observed drug protein interaction was not modeled. In the model the K_D value for BRAF is also used for BRAF(G466R), and the K_D value for BRAF(V600E) is also used for BRAF(V600D) and BRAF(V600K). Klaeger et al. (2017) did not distinguish between different phosphorylation states.

		K _D [nM]		
Entrez Gene Symbol	Kinase	Klaeger2017	Davis2011	Our model
		CHIR-265/RAF-265		
ABL1	ABL1-nonphosphorylated	n.i.	300	300
ABL1	ABL1-phosphorylated	n.i.	3600	--
BRAF	BRAF	n.i.	1200	1200
BRAF	BRAF(V600E)	n.i.	330	330
RAF1	RAF1	n.i.	390	390
SRC	SRC	n.i.	1100	1100
		Erlotinib		
ABL1	ABL1-nonphosphorylated	4327	330	330
ABL1	ABL1-phosphorylated	4327	76	--
EGFR	EGFR	2164	0.67	0.67
ERBB2	ERBB2	n.i.	2900	2900
ERBB3	ERBB3	n.i.	1100	1100
ERBB4	ERBB4	n.i.	230	230
GRB2	GRB2	2134	n.d. / n.i.	--
MAP3K1	MAP3K1	2247	n.d.	--
SRC	SRC	n.i.	700	700
		Lapatinib		
EGFR	EGFR	51	2.4	2.4
ERBB2	ERBB2	n.i.	7	7
ERBB3	ERBB3	n.i.	5500	--
ERBB4	ERBB4	n.i.	54	54
MAP2K7	MKK7	n.i.	4400	4400
		Vandetanib		
ABL1	ABL1-nonphosphorylated	1183	48	48
ABL1	ABL1-phosphorylated	1183	16	--
EGFR	EGFR	3741	9.5	9.5
ERBB2	ERBB2	n.i.	2600	2600
ERBB3	ERBB3	n.i.	160	160
ERBB4	ERBB4	n.i.	480	480
GRB2	GRB2	1003	n.d. / n.i.	--
MAP2K1	MEK1	n.i.	1800	1800
MAP2K2	MEK2	n.i.	1100	1100
SRC	SRC	n.i.	70	70
		Selumetinib		
EGFR	EGFR	n.i.	7000	7000
MAP2K1	MEK1	41	99	99
MAP2K2	MEK2	52	530	530
		PLX-4720		
ABL1	ABL1-nonphosphorylated	X	460	--
ABL1	ABL1-phosphorylated	X	2300	--
BRAF	BRAF	X	330	330
BRAF	BRAF(V600E)	X	100	100
MAP2K1	MEK1	X	550	--
MAP2K2	MEK2	X	1100	--
MAP2K4	MEK4	X	190	--
PAK1	PAK1	X	1400	--
RAF1	RAF1	X	170	--
SRC	SRC	X	4700	--
		PD0325901		
		Klaeger2017	Barrett2008	Our model
MAP2K1	MEK1	12	IC50: 0.33nM	0.33
MAP2K2	MEK2	12	IC50: 0.33nM	0.33